Dual-channel, single-photon upconversion detector at 1.3 μm

J. S. Pelc,[1,4,*] Paulina S. Kuo,[2,3,4,5] Oliver Slattery,[2] Lijun Ma,[2] Xiao Tang,[2] and M. M. Fejer[1]

[1]E. L. Ginzton Laboratory, Stanford University, Stanford, California 94305, USA
[2]Information Technology Laboratory, National Institute of Standards and Technology, Gaithersburg, Maryland 20899, USA
[3]Joint Quantum Institute, National Institute of Standards & Technology and University of Maryland, Gaithersburg, Maryland 20899, USA
[4] These authors contributed equally to this work
[5]paulina.kuo@nist.gov
[*]jpelc@stanford.edu

Abstract: We demonstrate a two-channel, upconversion detector for counting 1300-nm-wavelength photons. By using two pumps near 1550 nm, photons near 1300 nm are converted to two spectrally distinct channels near 710 nm using sum-frequency generation (SFG) in a periodically poled $LiNbO_3$ (PPLN) waveguide. We used spectral-conversion engineering to design the phase-modulated PPLN waveguide for simultaneous quasi-phasematching of two SFG processes. The two channels exhibit 31% and 25% full-system photon detection efficiency, and very low dark count rates (650 and 550 counts per second at a peak external conversion efficiency of 70%) through filtering using a volume Bragg grating. We investigate applications of the dual-channel upconversion detector as a frequency-shifting beamsplitter, and as a time-to-frequency converter to enable higher-data-rate quantum communications.

©2012 Optical Society of America

OCIS codes: (040.5570) Quantum detectors; (190.4410) Nonlinear optics, parametric processes; (270.5565) Quantum communications.

References and links

1. A. P. Vandevender and P. G. Kwiat, "High efficiency single photon detection via frequency up-conversion," J. Mod. Opt. **51**(9–10), 1433–1445 (2004).
2. M. A. Albota and F. N. C. Wong, "Efficient single-photon counting at 1.55 microm by means of frequency upconversion," Opt. Lett. **29**(13), 1449–1451 (2004).
3. C. Langrock, E. Diamanti, R. V. Roussev, Y. Yamamoto, M. M. Fejer, and H. Takesue, "Highly efficient single-photon detection at communication wavelengths by use of upconversion in reverse-proton-exchanged periodically poled $LiNbO_3$ waveguides," Opt. Lett. **30**(13), 1725–1727 (2005).
4. L. Ma, O. Slattery, and X. Tang, "Experimental study of high sensitivity infrared spectrometer with waveguide-based up-conversion detector(1)," Opt. Express **17**(16), 14395–14404 (2009).
5. J. S. Pelc, L. Ma, C. R. Phillips, Q. Zhang, C. Langrock, O. Slattery, X. Tang, and M. M. Fejer, "Long-wavelength-pumped upconversion single-photon detector at 1550 nm: performance and noise analysis," Opt. Express **19**(22), 21445–21456 (2011).
6. R. H. Hadfield, "Single-photon detectors for optical quantum information applications," Nat. Photonics **3**(12), 696–705 (2009).
7. M. D. Eisaman, J. Fan, A. Migdall, and S. V. Polyakov, "Invited Review Article: Single-photon sources and detectors," Rev. Sci. Instrum. **82**(7), 071101 (2011).
8. A. E. Lita, A. J. Miller, and S. W. Nam, "Counting near-infrared single-photons with 95% efficiency," Opt. Express **16**(5), 3032–3040 (2008).
9. H. Takesue, S. W. Nam, Q. Zhang, R. H. Hadfield, T. Honjo, K. Tamaki, and Y. Yamamoto, "Quantum key distribution over a 40-dB channel loss using superconducting single-photon detectors," Nat. Photonics **1**(6), 343–348 (2007).
10. H. Xu, L. Ma, A. Mink, B. Hershman, and X. Tang, "1310-nm quantum key distribution system with up-conversion pump wavelength at 1550 nm," Opt. Express **15**(12), 7247–7260 (2007).
11. L. Ma, J. C. Bienfang, O. Slattery, and X. Tang, "Up-conversion single-photon detector using multi-wavelength sampling techniques," Opt. Express **19**(6), 5470–5479 (2011).

12. A. P. VanDevender and P. G. Kwiat, "Quantum transduction via frequency upconversion," J. Opt. Soc. Am. B **24**(2), 295–299 (2007).
13. L. Ma, M. T. Rakher, M. J. Stevens, O. Slattery, K. Srinivasan, and X. Tang, "Temporal correlation of photons following frequency up-conversion," Opt. Express **19**(11), 10501–10510 (2011).
14. S. Tanzilli, W. Tittel, M. Halder, O. Alibart, P. Baldi, N. Gisin, and H. Zbinden, "A photonic quantum information interface," Nature **437**(7055), 116–120 (2005).
15. H. Takesue, "Erasing distinguishability using quantum frequency up-conversion," Phys. Rev. Lett. **101**(17), 173901 (2008).
16. M. T. Rakher, L. Ma, O. Slattery, X. Tang, and K. Srinivasan, "Quantum transduction of telecommunications-band single photons from a quantum dot by frequency upconversion," Nat. Photonics **4**(11), 786–791 (2010).
17. M. T. Rakher, L. Ma, M. Davanço, O. Slattery, X. Tang, and K. Srinivasan, "Simultaneous Wavelength Translation and Amplitude Modulation of Single Photons from a Quantum Dot," Phys. Rev. Lett. **107**(8), 083602 (2011).
18. M. Asobe, O. Tadanaga, H. Miyazawa, Y. Nishida, and H. Suzuki, "Multiple quasi-phase-matched $LiNbO_3$ wavelength converter with a continuously phase-modulated domain structure," Opt. Lett. **28**(7), 558–560 (2003).
19. P. Kumar, "Quantum frequency conversion," Opt. Lett. **15**(24), 1476–1478 (1990).
20. M. H. Chou, K. R. Parameswaran, M. M. Fejer, and I. Brener, "Multiple-channel wavelength conversion by use of engineered quasi-phase-matching structures in $LiNbO_3$ waveguides," Opt. Lett. **24**(16), 1157–1159 (1999).
21. Y. W. Lee, F. C. Fan, Y. C. Huang, B. Y. Gu, B. Z. Dong, and M. H. Chou, "Nonlinear multiwavelength conversion based on an aperiodic optical superlattice in lithium niobate," Opt. Lett. **27**(24), 2191–2193 (2002).
22. K. R. Parameswaran, R. K. Route, J. R. Kurz, R. V. Roussev, M. M. Fejer, and M. Fujimura, "Highly efficient second-harmonic generation in buried waveguides formed by annealed and reverse proton exchange in periodically poled lithium niobate," Opt. Lett. **27**(3), 179–181 (2002).
23. Excelitas Technologies, "SPCM-AQRH: Single Photon Counting Module," http://www.excelitas.com/downloads/DTS_SPCM_AQRH.pdf
24. K. J. Gordon, V. Fernandez, G. S. Buller, I. Rech, S. D. Cova, and P. D. Townsend, "Quantum key distribution system clocked at 2 GHz," Opt. Express **13**(8), 3015–3020 (2005).
25. J. C. Bienfang, A. Restelli, and A. Migdall, "SPAD electronics for high-speed quantum communications," Proc. SPIE **7945**, 79452N, 79452N-5 (2011).
26. P. A. Andrekson and M. Westlund, "Nonlinear optical fiber based high resolution all-optical waveform sampling," Laser Photon. Rev. **1**(3), 231–248 (2007).
27. O. Kuzucu, F. N. C. Wong, S. Kurimura, and S. Tovstonog, "Time-resolved single-photon detection by femtosecond upconversion," Opt. Lett. **33**(19), 2257–2259 (2008).
28. J. Huang, C. Langrock, X. P. Xie, and M. M. Fejer, "Monolithic 160 Gbit/s optical time-division multiplexer," Opt. Lett. **32**(16), 2420–2422 (2007).
29. W. Robert, Boyd, *Nonlinear Optics,* 2nd ed. (Academic Press, 2003).
30. J. R. Kurz, J. Huang, X. Xie, T. Saida, and M. M. Fejer, "Mode multiplexing in optical frequency mixers," Opt. Lett. **29**(6), 551–553 (2004).
31. B. H. Kolner and M. Nazarathy, "Temporal imaging with a time lens," Opt. Lett. **14**(12), 630–632 (1989).
32. B. H. Kolner, "Space-time duality and the theory of temporal imaging," IEEE J. Quantum Electron. **30**(8), 1951–1963 (1994).
33. C. V. Bennett and B. H. Kolner, "Principles of Parametric Temporal Imaging —Part I: System Configurations," IEEE J. Quantum Electron. **36**(4), 430–437 (2000).
34. C. Niclass, C. Favi, T. Kluter, M. Gersbach, and E. Charbon, "A 128 × 128 Single-Photon Image Sensor with Column-Level 10-Bit Time-to-Digital Converter Array," IEEE J. Solid-state Circuits **43**(12), 2977–2989 (2008).

1. Introduction

Single-photon upconversion detectors for counting 1.3- and 1.5-μm-wavelength photons are attractive alternatives to direct detection by either InGaAs avalanche photodiodes (APDs) or superconducting single-photon detectors (SSPDs). The 1.3- and 1.5-μm wavelengths are of interest for optical-fiber-based quantum communication systems as silica fibers have minimum attenuation in these wavelength windows. Upconversion detection is based on highly efficient sum-frequency generation (SFG) that converts near-infrared photons to shorter-wavelength photons that can be detected by Si APDs, which offer higher detection efficiencies and lower dark count rates than their InGaAs-based counterparts [1–5]. InGaAs APDs are generally gated to reduce dark counts and avoid after-pulsing, which may also limit the speed at which events can be detected. SSPDs can also be used to detect near-infrared photons with very good sensitivity and dark count rates [6–9], but they require cryogenic operating temperatures, and are therefore of limited utility in practical quantum communications systems.

Upconversion detectors have been used for a number of applications. Improved system performance of a quantum key distribution system has been shown using 1306-nm

upconversion detectors [10]. Multiwavelength sampling using an upconversion detector has been used to increase temporal resolution of the detector system [11]. The upconversion process has been shown to preserve phase coherence [12] and temporal correlations up to fourth order [13]. Frequency upconversion has enabled a quantum information interface between widely separated wavelengths [14] and erasing of frequency distinguishability between two single photons [15]. Upconversion is a useful tool for hybrid quantum systems such as those combining quantum dots with photonic qubits [16, 17].

Here, we demonstrate a single-photon upconversion detector that has two spectrally distinct channels. Through quasi-phasematching (QPM) and spectral-conversion engineering [18], we can achieve efficient upconversion to multiple wavelengths in a single periodically poled lithium niobate (PPLN) waveguide. Specifically, we engineer the PPLN waveguide for two simultaneous SFG processes: 1302 nm + 1556 nm $\rightarrow$ 709 nm and 1302 nm + 1571 nm $\rightarrow$ 712 nm. We observed 70% conversion efficiency for both channels in the PPLN waveguide (including waveguide coupling losses), which led to system photon-detection efficiencies greater than 25%. In addition to sensitive detection of 1.3-µm signal photons, such a device acts like a beamsplitter or demultiplexer for the signal photons. We explore applications of this additional functionality for improving system performance. We show higher count rates before the onset of saturation, and better timing resolution by using time- to wavelength-division multiplexing. Simultaneously, we show ultra-low dark count rates (<700 s^{-1} at peak conversion efficiency) for both channels by narrowband filtering using a volume Bragg grating.

2. Theory

Consider a waveguide in which the following SFG processes can be simultaneously quasi-phasematched:

$$
\begin{aligned}
\omega_0 + \omega_{p1} &= \omega_1 \\
\omega_0 + \omega_{p2} &= \omega_2 \quad . \\
&\;\;\vdots \\
\omega_0 + \omega_{pN} &= \omega_N
\end{aligned}
\tag{1}
$$

A single-photon signal at ω_0 can undergo simultaneous sum-frequency generation with N strong pumps at frequencies ω_{p1} to ω_{pN}. Considering the simplest, non-trivial case of $N = 2$, the coupled wave equations for the electric fields, a_j (normalized such that $|a_j|^2$ has units of photons per second), are

$$
\begin{aligned}
\frac{da_0}{dz} &= -\gamma_1 a_1 - \gamma_2 a_2 \\
\frac{da_1}{dz} &= \gamma_1 a_0 \qquad\qquad , \\
\frac{da_2}{dz} &= \gamma_2 a_0
\end{aligned}
\tag{2}
$$

where $\gamma_j = \sqrt{\eta_{\text{nor}} P_{pj}}$ and η_{nor} is the normalized efficiency defined in Ref [5]. The pumps at ω_{p1} and ω_{p2} are assumed to be undepleted (valid for the weak input signals considered here), both processes are phasematched (which can be achieved using a phase-modulated QPM grating described below), and the propagation losses are negligible. By taking the second derivative with respect to z of the first equation and substituting the second two expressions, we obtain

$$\frac{d^2 a_0}{dz^2} = -(\gamma_1{}^2 + \gamma_2{}^2) a_0 . \qquad (3)$$

Substituting $\Gamma = \sqrt{\gamma_1{}^2 + \gamma_2{}^2}$, this equation is solved by

$$a_0(z) = A \cos \Gamma z + B \sin \Gamma z . \qquad (4)$$

We solve the remaining two equations and insert the initial conditions $a_0(0)$, $a_1(0)$, and $a_2(0)$ to yield:

$$\begin{aligned}
a_0(L) &= a_0(0) \cos \Gamma L - [\bar{\gamma}_1 a_1(0) + \bar{\gamma}_2 a_2(0)] \sin \Gamma L, \\
a_1(L) &= \bar{\gamma}_1 a_0(0) \sin \Gamma L + [\bar{\gamma}_1{}^2 a_1(0) + \bar{\gamma}_1 \bar{\gamma}_2 a_2(0)] \cos \Gamma L + \bar{\gamma}_2{}^2 a_1(0) - \bar{\gamma}_1 \bar{\gamma}_2 a_2(0), \qquad (5) \\
a_2(L) &= \bar{\gamma}_2 a_0(0) \sin \Gamma L + [\bar{\gamma}_1 \bar{\gamma}_2 a_1(0) + \bar{\gamma}_2{}^2 a_2(0)] \cos \Gamma L - \bar{\gamma}_1 \bar{\gamma}_2 a_1(0) + \bar{\gamma}_1{}^2 a_2(0)
\end{aligned}$$

where $\bar{\gamma}_j = \gamma_j / \Gamma$ are the normalized coupling constants. Equation (5) can be easily generalized for N pumps where $\Gamma = \left(\sum_j \gamma_j{}^2 \right)^{1/2}$ and $\sum_j \bar{\gamma}_j{}^2 = 1$.

In an ideal device with no loss and $a_1(0) = a_2(0) = 0$, complete signal-photon conversion is obtained when $\Gamma L = \pi/2$. For the trivial case of one strong pump, 100% conversion is achieved when the pump power is $P_p = \pi^2 / 4\eta_{nor} L^2$ and corresponds to the case when one photon at ω_0 is annihilated to produce one photon at the sum frequency ω_1. For multiple pumps at 100% conversion, a single photon at ω_0 is annihilated while a sum-frequency photon at ω_j is produced with probability $\bar{\gamma}_j{}^2$. The multi-channel upconverter acts like a beamsplitter that routes the signal photon to N possible outputs corresponding to different frequencies ω_j. The splitting ratio is variable and depends on the choice of pump power for each channel. At $\Gamma L = \pi/2$, the device behaves as a quantum frequency converter [19] that translates the quantum properties of the photons at ω_0 to photons at ω_j.

In real-world devices, there are losses and incomplete conversion. For quantum information applications, the effects of loss and incomplete conversion are similar. The key exchange rate in a quantum key distribution system is reduced by system losses, whether they result from link losses, detector inefficiencies or incomplete upconversion. The effect of loss on two-photon interference measurements (which are the basis for many quantum entanglement experiments) is to reduce visibility and increase background noise counts, but the correlation signature is preserved. The multi-channel upconverter acts like a lossy beamsplitter where incomplete conversion contributes to the system loss.

3. QPM design and fabrication

To fabricate a multichannel upconversion device, we employed the QPM phase-modulation technique developed by Asobe and associates [18]. The phase-modulation technique is one of several techniques [20, 21] that have been developed in order to engineer the phasematching profile of a device. In the phase-modulation technique, one starts with a QPM grating with period Λ_G. The QPM pattern is modulated by a phase-modulation function $\phi(z)$ that is periodic in z with period Λ_{ph}. The phase modulation consist of shifting position of a domain boundary z_n with respect to its nominal location $z_{n,0}$ of a periodic grating so that the modulation phase is $\phi(z) = 2\pi(z_n - z_{n,0})/\Lambda_G$. Using Fourier analysis, it can be shown that QPM peaks are obtained when the relation

$$\Delta k = k_j - k_0 - k_{pj} = 2\pi \left(\frac{1}{\Lambda_G} + \frac{m}{\Lambda_{ph}} \right) \qquad (6)$$

is satisfied for integer m. k_j, k_0, and k_{pj} are the wavevectors for sum-frequency ω_j, signal ω_0, and pump ω_{pj}, respectively. We used a simplex convex optimization algorithm to successfully optimize $\phi(z)$ to phasematch two simultaneous SFG processes corresponding to $m = +1$ and -1; for the two-peaked QPM tuning curve, the desired form of $\phi(z)$ is found to be a rectangle function. A calculated QPM tuning curve is shown in Fig. 1a. We found that Λ_{ph} varied inversely with the wavelength difference between the two QPM peaks. We computed the Δk values from simulated dispersion data for reverse-proton exchange (RPE) [22] PPLN waveguides. Setting $m = +1$ and -1 in Eq. (6), we can solve for the required poling period Λ_G and phase-modulation period Λ_{ph} for a given pair of wavelengths. For channel separations (defined as $\Delta\lambda = \lambda_{p2} - \lambda_{p1}$) of 5, 10, and 15 nm, we found that the required phase-modulation periods Λ_{ph} were 7.1, 3.94, and 2.56 µm, respectively.

We fabricated two-channel upconversion RPE PPLN waveguides for SFG between a 1.3-µm signal and two 1.55-µm-band pumps, with $\Lambda_G = 13.5$ µm. The 52-mm-long devices were antireflection coated for wavelengths of 1310 and 1550 nm at the input between LiNbO$_3$ and optical fiber, and for 1310, 1550, and 710 nm at the output between LiNbO$_3$ and air. The devices were fiber pigtailed at the inputs and were measured to have total optical throughputs of -1.3 dB at 1550 nm and -2.4 dB at 1319 nm. The tuning curve vs. pump wavelength of a device measured with the signal wavelength fixed to $\lambda_0 = 1319$ nm is shown in Fig. 1b. The conversion efficiencies of the two channels (at 1533 nm and 1548 nm pump wavelengths) are nearly equal. Lower-efficiency side peaks for odd m were also observed, which are a consequence of the phase-modulation design.
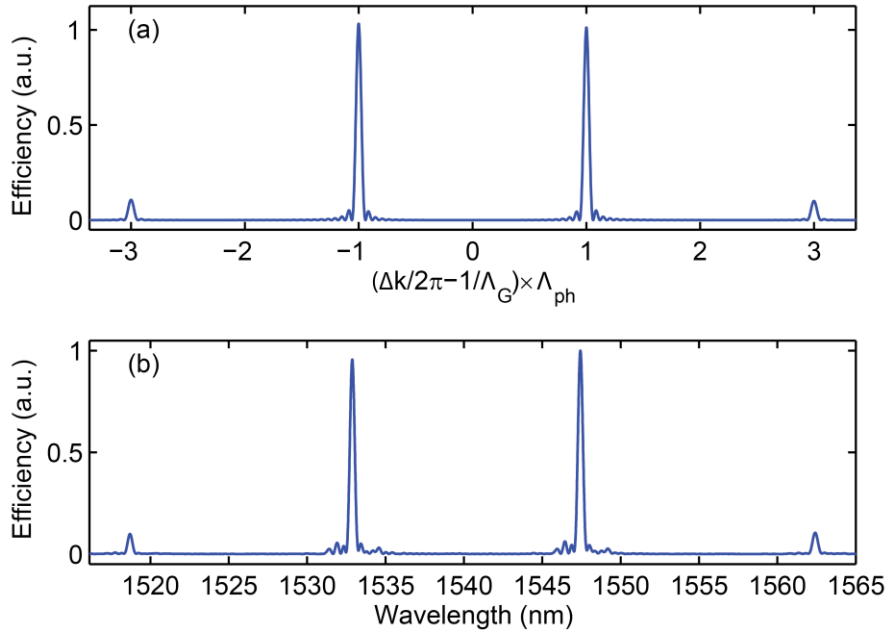

Fig. 1. (a) Theoretical and (b) measured SFG conversion efficiency for the two-channel, phase-modulated PPLN waveguide with signal wavelength fixed at $\lambda_0 = 1319$ nm.

4. Experiments

We first characterized the performance of each channel of the upconversion detector by measuring the photon detection efficiency (PDE) and dark count rate (DCR) using continuous wave (CW) pumping. We then explored the multiplexing capabilities of the device for several applications. These applications can be separated into two categories: use of the multi-channel device as a beamsplitter and as a switch. We used the dual channel device as a beamsplitter to exceed the saturation-limited maximum count rate of a single detector. Using the device as a switch, we demonstrated increased clock rate above the jitter-limited clock rate of a single-channel upconversion detection system.

4.1 Photon detection efficiency and dark counts

A diagram of the experimental setup is shown in Fig. 2. In order to pump both upconversion channels simultaneously, two pump lasers were used: one in the C-band ($\lambda < 1568$ nm) and one in the L-band ($\lambda > 1568$ nm). The two pumps were combined with a C/L-band wavelength division multiplexer (WDM) and amplified in a 0.5W erbium-doped fiber amplifier (EDFA). The EDFA was followed by a 1300/1550 WDM acting as a filter to reject 1310-nm noise produced in the EDFA, as has been described in Ref [4]. The amplified pumps were combined with a 1310-nm signal laser attenuated down to single-photon-level and sent into the fiber-pigtailed, phase-modulated PPLN waveguide. Polarization controllers were used for both pumps and the signal to align the input light to the z-axis of the PPLN waveguide, which supports only e-polarized light.
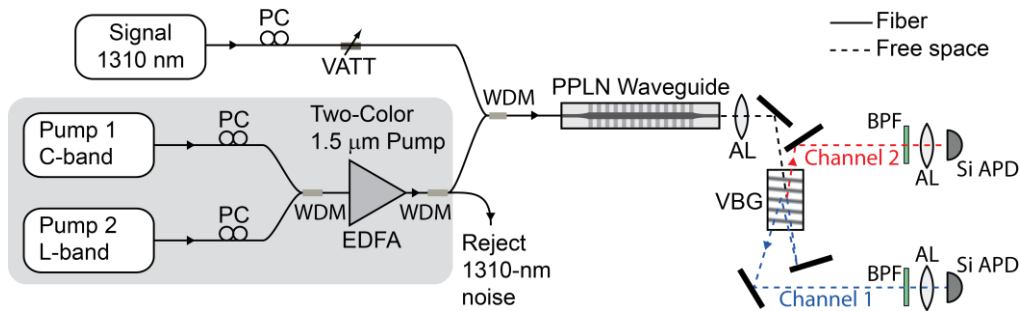

Fig. 2. General experimental setup. The strong, two-color pump near 1.5 μm is combined with the signal near 1310 nm in the PPLN waveguide with phase-modulated QPM grating. The output is separated by a volume Bragg grating (VBG) and sent to two silicon avalanche photodiodes (Si APD). PC, polarization controller; WDM, wavelength-division multiplexer; EDFA, erbium-doped fiber amplifier; VATT, variable attenuator; AL, aspheric lens; BPF, 20-nm band-pass filter.

Following the waveguide, an anti-reflection-coated aspheric lens (AL) was used to collimate the output radiation from the waveguide. To separate the outgoing pump light and filter the two up-converted channels at λ_1 and λ_2, we used a volume Bragg grating (VBG). In reflection, the VBG acts as a narrowband filter, where the reflected wavelength depends sensitively on the angle of incidence. We measured the full-width-half-maximum (FWHM) reflection bandwidth of the VBG to be 0.04 nm. The VBG was aligned such that the long-wavelength channel at λ_2 was reflected back through the input facet of the VBG (see Fig. 2). The upconverted light at λ_1 passed through the VBG and was redirected back into the VBG using a mirror at a slight angle so that high reflection of λ_1 was achieved through the second surface of the VBG. One key advantage of using the VBG filter compared to an earlier approach using a holographic diffraction grating [11] is that narrowband wavelength selectivity, and therefore very low noise counts, can be achieved using a very small footprint. The two upconverted channels were then sent to two Si APDs (PerkinElmer SPCM-AQR-14). We used a 20-nm bandpass filter at the entrance to each Si APD to block any stray light or parasitic pump-second-harmonic radiation. An unintended consequence of the phase-

modulated QPM design was the appearance of several accidental second-harmonic generation QPM peaks. We chose the pump wavelengths, λ_{p1} and λ_{p2}, such that these undesired peaks were avoided.

The measured CW system photon detection efficiencies and dark count rates for both channels are shown in Fig. 3. The PDEs and DCRs were measured with only one pump present at a time. The signal wavelength was fixed to 1302 nm so that channel 1 corresponded to the SFG process 1302 nm + 1556 nm → 709 nm, while channel 2 corresponded to 1302 nm + 1571 nm → 712 nm. For the PPLN waveguide itself, we observed 70% peak external conversion efficiency in both channels, a value which included input and output coupling losses. The optical path following the PPLN waveguide had higher loss for channel 1 than channel 2, primarily due to traversing the VBG twice; we estimated 45% and 32% loss for the optical path after the waveguide for channel 1 and 2, respectively, which includes loss from the 20-nm band-pass filter. Combined with the 65% PDE of the Si APD [23], the system peak photon detection efficiencies were 25% for channel 1 and 31% for channel 2 (see Fig. 3a). The solid lines in Fig. 3a represent fits to $\eta_{tot}(P_p) = \eta_0 \sin^2(\pi/2\sqrt{P_p/P_{max}})$, where η_{tot} is the PDE, P_p is the pump power, and P_{max} is the pump power at maximum conversion. $P_{max} \approx 135$ mW is nearly the same for channels 1 and 2, as we expected from the nearly equal peak heights in Fig. 1b.

At maximum conversion, the dark count rates are 550 s^{-1} and 650 s^{-1} for channels 1 and 2, respectively. The DCRs at low pump power are dominated by the intrinsic DCRs of the Si APDs. The dark count rates observed here represent substantial improvements compared to other CW 1.3-µm-band upconversion detectors that showed 1.5×10^4 s^{-1} [3] and 2.5×10^3 s^{-1} [4] DCRs. Our low DCRs are due to the very narrowband reflectance of the VBG. In this system, the noise is primarily due to upconverted anti-Stokes Raman photons generated by the strong pump, which fill the PPLN upconversion acceptance bandwidth [3–5]. The VBG acts as a filter narrower than the QPM acceptance bandwidth, so that most of the noise photons are eliminated. There is a tradeoff between system speed and noise performance. The narrow VBG (24 GHz) and QPM acceptance (46 GHz) bandwidths set a limit to the response rate of the system; broadening both of these bandwidths would allow faster rates at the expense of greater total noise counts.
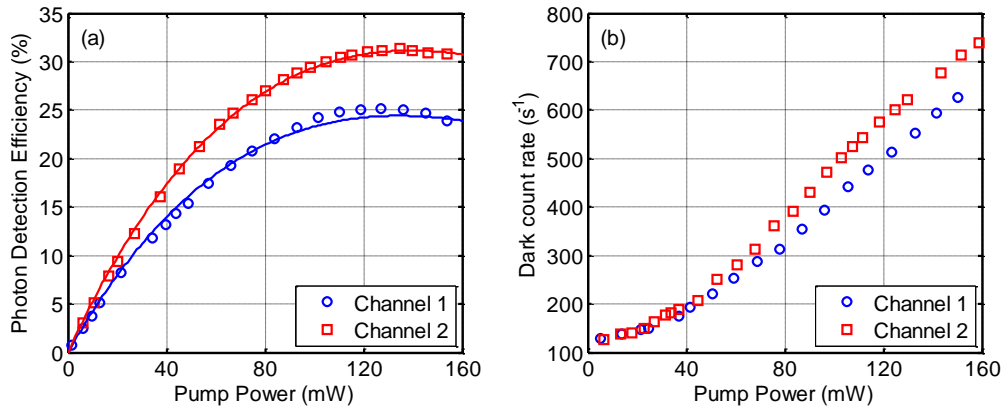

Fig. 3. Measured (a) photon detection efficiencies and (b) dark count rates for channel 1 (1302 nm + 1556 nm → 709 nm) and channel 2 (1302 nm + 1571 nm → 712 nm). The intrinsic dark count rates of the Si APDs are about 100 s^{-1}.

4.2 Classical beamsplitter applications

When both pump frequencies are present at the same time, the dual-channel upconverter with VBG output filter acts like a classical beamsplitter that probabilistically divides the input to two outputs. Photons at 1302 nm are frequency-converted by the device and sent to the 709- or 712-nm output paths. Beamsplitters have many uses in quantum optics. We demonstrated application of our device for splitting high-count-rate signals onto two Si APDs to enable single-photon count rates above the dead-time-limited value of a single detector.

The maximum count rate of an APD is related to the dead time of the detector, τ_D. As the incident photon rate R_{inc} begins to approach $1/\tau_D$, the detector begins to saturate [23]. Consider a single photon at ω_0 incident at the input of the dual-channel upconverter device. The pump powers P_{p1} and P_{p2} can be chosen such that with 50% probability, the photon is converted to ω_1 or ω_2. Therefore, much like a classical beamsplitter, the dual-channel upconverter will probabilistically divide the incident 1.3-µm signal to the two upconverted channels that can be detected by two APDs.

We measured the saturation of a Perkin-Elmer SPCM by varying R_{inc} and measuring the count rate R of a single detector (Fig. 4). The input signal rate R_{inc} at $\lambda_0 = 1302$ nm was controlled by a programmable optical attenuator in 2 dB increments from a level of 41 photons/s to 2×10^9 photons/s. With only pump 1 turned on, we measured the count rates for both channels (R_1 and R_2). R_2 was very low and reflected detector dark counts and cross-talk counts. The count rate R_1 is shown as blue circles in Fig. 4. The solid blue curve is a simulation of the expected counting statistics of coherent light (with Poissonian photon arrival statistics) assuming a detector dark count rate $D = 250$ s^{-1} and a dead time of 67 ns. By comparing the rates R_1 and R_2 with only pump 1 turned on, we observed a very low channel crosstalk of −44 dB, which is likely due to a combination of amplified spontaneous emission (ASE) from the EDFA and imperfect isolation of the VBG channels.

With both pumps turned on, we then set the pump powers P_{p1} and P_{p2} such that, including free-space losses, equal count rates were obtained at the two detectors. We measured the summed count rate $R_s = R_1 + R_2$ at the same overall conversion efficiency as in the pump-1-only case. The observed R_s versus R_{inc} is plotted as green squares in Fig. 5, along with a simulation of the counting statistics. We see that at low R_{inc}, the dual-channel case has a DCR
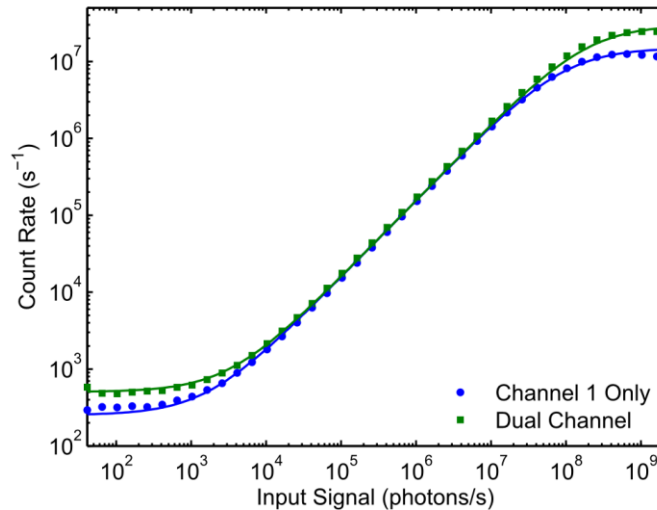

Fig. 4. Measured count rates for a single detector (blue dots) and a combined, dual-channel detector (green squares) as a function of input signal rate R_{inc}. The maximum, saturated count rate for the dual-channel system is twice that of the single detector, but the dark count rate is also doubled. The solid curves are simulated counting statistics for coherent light.

of approximately $2D$ and saturates at $2R_{max}$, where D is the DCR for a single channel and R_{max} is the maximum, dead-time-limited count rate obtained with one detector. From this result, we extrapolate that for an N-pump upconverter, the system count rate would saturate at NR_{max} at the expense of increased DCR of ND.

4.3 Demultiplexing applications

In the previous section, we discussed application of a multichannel upconverter as a classical beamsplitter when the pump sources are simultaneously on. In that demonstration, the splitting of an input signal to multiple output ports happened probabilistically. If, however, the two pumps were controlled in time using external modulators, one may achieve deterministic control of the output channel for a particular time bin by, for example, switching the pumps on and off sequentially. Such a multichannel detector can be used to switch the output from one channel to another like a router or demultiplexer. One application of such functionality is to achieve higher speeds by using multiple Si APDs.

High speed detectors are of interest for quantum key distribution (QKD) systems. The exchange rate of the secret key is much slower than the system clock rate due to post-selection protocols [24, 25]. The quantum-key transmission rate is further reduced by losses and other errors, especially in long-distance transmission systems. Hence, increasing the system clock rate can enable faster QKD systems over longer distances. The speed limitation for such systems is typically caused by the detectors. For a system based on upconversion detection using a continuous-wave pump, timing jitter in the Si APD limits the temporal resolution. Pulsed pumps can be used to increase the temporal resolution. Picosecond [26] and femtosecond [27] pump pulses generated by mode-locked lasers have been used to demonstrate fast optical sampling. However, these schemes are based on varying the delay of the sampling pulse and collecting data over a number of repeated waveforms, which is not possible in a communications system. Alternatively, the pump pulses can be used to demultiplex a fast data train into multiple slower trains that can be resolved with slower detectors. Such a scheme is analogous to a frequency-converting, optical time-division multiplexer [28], which was used to quadruple the data rate by combining four wavelength channels.

High-speed upconversion detection using time- to wavelength-division multiplexing has previously been demonstrated using a short, PPLN waveguide [11]. The 1-cm waveguide used in Ref [11]. was chosen to permit two spectrally distinct pumps to fit under the same phasematching peak. The FWHM pump-acceptance bandwidth was 2.5 nm centered at 1549.6 nm, which allowed the use of pumps at 1549.2 nm and 1550.0 nm, but produced low conversion efficiency due to the 1-cm length of the QPM grating. One major advantage of the phase-modulated PPLN waveguide used here is the higher photon detection efficiency for both channels. Our 52-mm-long device showed up to 31% system PDE (see Fig. 4a) while the 10-mm-long waveguide in Ref [11]. had only 7% maximum PDE, limited by the available pump power. We were able to reach the point of maximum signal conversion at 135 mW pump power, while Ref [11]. had insufficient pump power to reach the maximum conversion point. The phase-modulated QPM technique used here can provide a scalable approach to increase the number of channels. High conversion efficiency for each channel is obtained without decreasing channel spacing, which would make the spectral filtering of the output channels more difficult.

The dual-channel device allows access to higher data rates. Let τ_{det} be the shortest time bin allowed by a Si APD while still maintaining acceptably low inter-symbol interference (ISI); using the dual-channel upconversion device, a faster train of signal pulses with time bin $\tau_{det}/2$ can enter the device and interact with a two-color pump consisting of interleaved pumps pulses at λ_{p1} and λ_{p2}. The period of the pump pulses at each wavelength is τ_{det}. A train of upconverted pulses is generated in the PPLN waveguide, where pulses in adjacent time slots have different wavelengths, which can be spectrally separated using a dispersive optic (here, a VBG) and sent to two Si APDs. The phase-modulated PPLN waveguide and VBG together act like a time-division demultiplexer that produces two trains of pulses, each at half the

signal clock rate. The dual-channel upconverter therefore allows detection of a train of signal pulses whose rate is twice larger than the detector-limited rate ($1/\tau_{det}$).

A detailed diagram of the experimental setup is shown in Fig. 5. The two pumps and signal are modulated by electro-optic intensity modulators (IMs) using the timing diagram shown in Fig. 6 (with 1.6 GHz clock rate). The electrical pulses driving the IMs are produced with a data generator, which is also used to trigger the time-correlated single-photon counting (TCSPC) system. The optical pulses are combined and sent to the phase-modulated PPLN waveguide. The two-color SFG output is filtered and separated with the VBG and detected with two Si APDs.
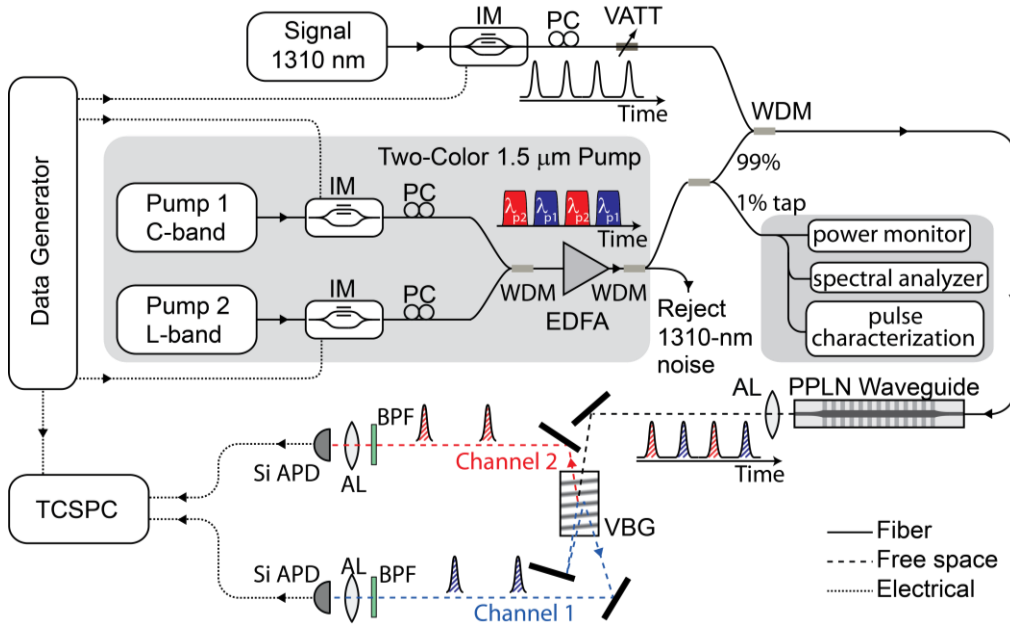

Fig. 5. Experimental setup for the dual-wavelength demultiplexing experiment. A fast train of signal pulses interacts in the PPLN waveguide with a two-color pump pulse train consisting of alternating pulses at λ_{p1} and λ_{p2} to produce SFG pulses that can be spectrally separated with the VBG. The pulses arrive at each Si APD at half the rate of the original signal pulse train. A data generator drives the electro-optic intensity modulators (IM) and also triggers the time-correlated single-photon counting (TCSPC) system. A 1% tap coupler is placed after the EDFA and used to monitor the power, optical spectrum and temporal characteristics of the pump pulses. The resulting dual-channel SFG pulses are separated and filtered by the VBG and routed to two Si APDs.
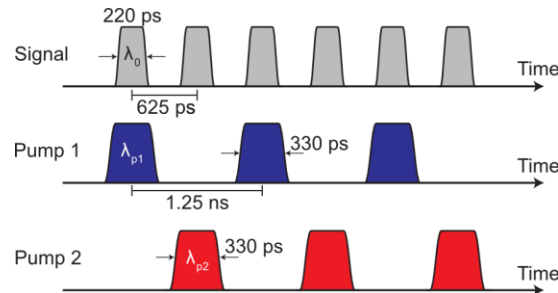

Fig. 6. Pulse timing diagram for detection of high-clock-rate signals via multi-wavelength sampling. The signal pulses have 625 ps period (1.6 GHz rate), while the two pump pulse trains each have 1.25-ns period (800 MHz rate). The pump pulse trains are staggered such that signal pulses overlap with alternating pump pulses.

We first measured the timing jitter of a single APD. This was done by sending pump and signal pulses (of FWHM 330 ps and 220 ps, respectively) to the PPLN waveguide once every 12.5 ns. With widely spaced pulses, the tails of the detected SFG can be easily distinguished (see Fig. 7a, green dots). We observed FWHM of 310 ps and full-width at 1% maximum (FW1%M) of 1.0 ns. The floor of background counts around −33 dB is due to residual pump and signal transmission from imperfect extinction of the electro-optic modulators.

The black dots in Fig. 7a show the upconverted signal with signal pulses arriving at 1.6 GHz and a continuous-wave pump. We see ISI such that adjacent time slots cannot be well distinguished. By using the dual-wavelength upconversion device and pulsing the two pumps according to the timing diagram in Fig. 6, we obtain the timing histograms shown in Fig. 8b. The effective data rate in each channel is lowered to 800 MHz, and there is much less inter-symbol interference and greater ease in distinguishing data in each channel.

As an example application for data transmission, we sent a test code sequence to the dual-wavelength upconversion detector (Fig. 8). The test sequence is encoded in the signal at λ_0 and shown in Fig. 8b, while the response histograms for channels 1 and 2 are plotted in Figs. 8a and 8c, respectively. Figure 8d shows the result of sending all the data to channel 1 (pump 1 is held continuously on); data in adjacent time slots are merged. When the signal data is "0," both channels show a small amount of feed-through (manifested as a small increase in counts at the center of the time bin), which is caused by incomplete extinction of the 1.3-μm signal intensity modulator.
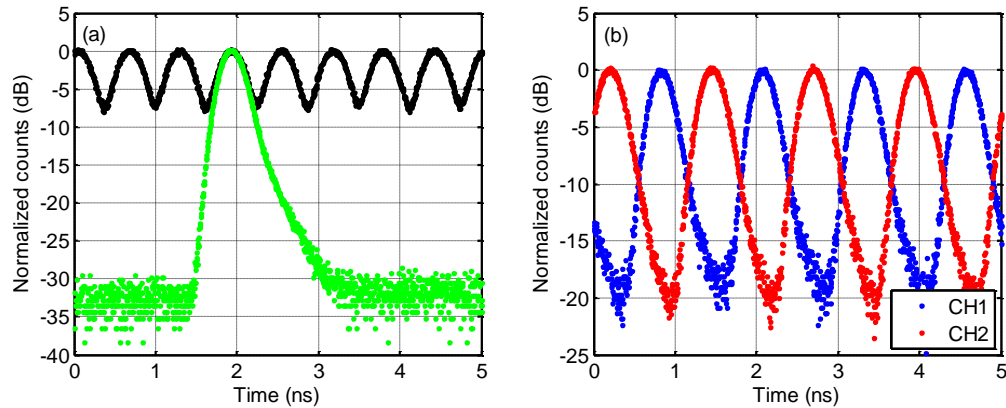
Fig. 7. (a). Single-channel, up-conversion detector response to a 1.6 GHz clock-rate pulse train showing significant inter-symbol interference (black), and response to a single pulse (green) showing FW1%M of 1.05 ns. (b) By using the dual-channel, upconversion detector and alternating channel 1 and 2 pumping, the data rate in each channel is halved and the data can be resolved.
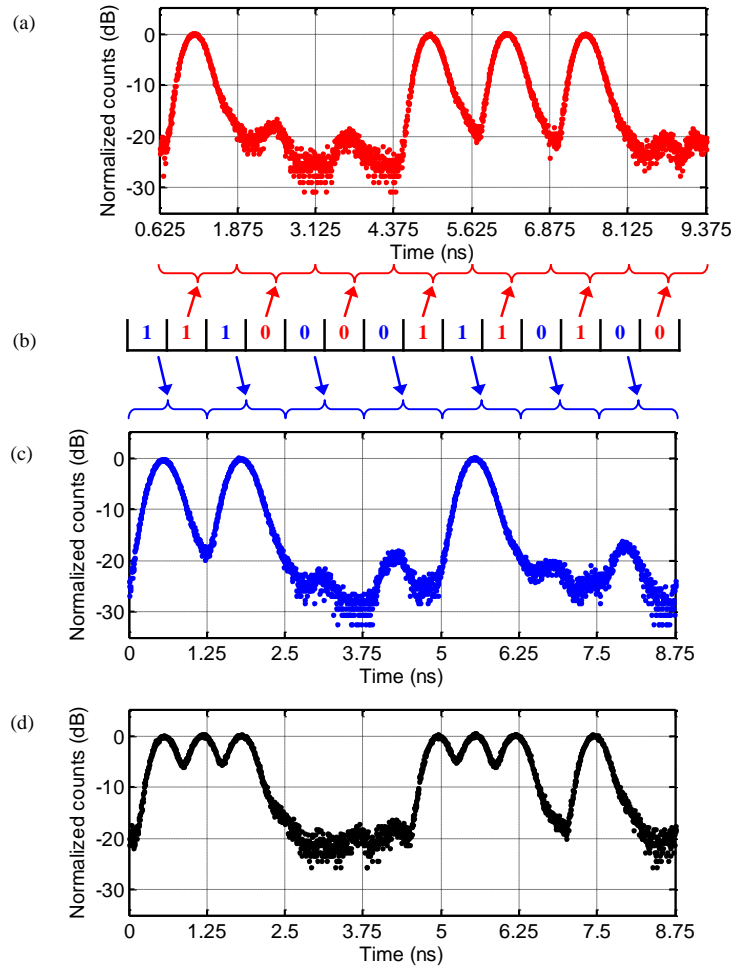
Fig. 8. Timing histogram of dual-wavelength upconversion detector for (a) Channel 1 and (c) Channel 2 to test sequence (b) encoded in the signal at λ_0. (d) Response of Channel 1 to the signal code sequence with a continuous-wave pump showing significant ISI.

5. Conclusion and future work

We have demonstrated a dual-wavelength, high-efficiency upconversion single-photon detector with extremely low dark count rates. The system is based on a PPLN waveguide with a phase-modulated QPM grating where the output light is filtered by a volume Bragg grating. We measured total-system photon detection efficiencies (dark count rates) of 25% (550 s^{-1}) and 31% (650 s^{-1}) for channels 1 and 2, respectively. We showed that the dual-channel upconversion detector can be used both as a probabilistic beamsplitter and as a deterministic switch. When used as a beamsplitter, multiple Si APDs can be used to count the upconverted photons, thereby increasing the saturation-limited count rate. With pulsed pumping, the device worked as a router that deterministically switched the output from one channel to another. We showed an increase in clock rate beyond the rate limited by the timing jitter of a single Si APD. As a beamsplitter, we expect the dual-channel device to preserve photon statistics and enable g$^{(2)}$ measurements of classical and non-classical light. With more channels, higher order temporal correlation functions may be measured using the device. When used as a router, the dual-channel device is a fast switch whose switching time is only limited by the electro-optic modulators controlling the pumps since optical frequency

conversion is instantaneous [29]. We envision this technique may be useful as a rapid switch between measurement bases in a quantum key distribution system. While we have here used two pumps with different optical frequencies to switch between two output modes, it is also possible to use different spatial modes in combination with a mode-selective device to achieve the same switching functionality [30].

Multichannel upconversion and sampling are examples of discrete time-to-frequency conversion. There has been growing interest in time-to-frequency converters for their applications in time microscopes [31–33], where ultrafast waveforms can be magnified in time such that they can be detected directly using high speed electronics. An extension of the multiple discrete wavelength sampling presented here would be to investigate continuous wavelength sampling using a chirped pump pulse (with, for example, a linearly varying instantaneous frequency as a function of time) to upconvert a weak input signal with rapid temporal variations. Each temporal slice of the input waveform is linearly mapped onto the frequency of the upconverted light. If a diffraction grating or other dispersive element is used followed by a single-photon detector array [34], one can map each temporal slice of the input waveform onto an individual detector element, enabling potentially much higher timing resolution than that provided by an individual detector element. This technique is advantageous over the single-pixel, ultrafast upconversion approach studied in Ref [27], as it can sample the entire waveform in a single shot. Such a single-shot, high-time-resolution detector system would have applications in pulse-position-modulated, weak-pulse optical communications, where the time-to-frequency converter enables narrower temporal bin widths and higher data rates.

Acknowledgments